AERODYNAMICAL AND AEROELASTIC INVESTIGATIONS OF A RIBLET DESIGN APPLLIED ON THE SURFACE OF TURBINE EXIT GUIDE VANES OF A LOW PRESSURE TURBINE

M. Zenz[1], A. Hafizovic[1], L. Simonassi[1], P. Leitl[2], R. Benauer[2], F. Heitmeir[1] and A. Marn[1]

[1] Institute of Thermal Turbomachinery and Machine Dynamics, Graz University of Technology, Graz, Austria

[2] Bionic Surface Technologies GmbH, Graz, Austria

ABSTRACT

The present work gives a closer insight into the aerodynamic parameters obtained for turbine exit guide vanes (TEGV) of a low pressure turbine (LPT) with riblets applied on their suction side. Experimental data was obtained by using an aerodynamic five-hole-probe including a thermocouple as well as a trailing edge probe. Additionally, a comparison between the flow fields of the experimental data and the numerical results, obtained by performing a steady state Reynolds-Averaged Navier-Stokes (RANS) simulation, was done. The investigated flow fields are located up- and downstream of the TEGV's and show a good overall agreement.

Additionally, aeroelastic investigations show an influence of the changed surface structure onto the vibrations of the upstream located rotor blades. For a visual examination of the flow field, oil flow visualizations are performed and compared with results obtained by CFD simulations.

KEYWORDS

RIBLETS, LOW PRESSURE TURBINE, AERODYNAMICS, AEROELASTICS, TURBINE EXIT GUIDE VANES, CFD

NOMENCLATURE

Abbreviations

CFD	Computational Fluid Dynamics
LE	Leading Edge
LPT	Low Pressure Turbine
LPV	Lower Passage Vortex
MRF	Moving Reference Frame
PS	Pressure Side
RANS	Reynolds-Averaged Navier-Stokes
SS	Suction Side
STTF-AAAI	Subsonic Test Turbine Facility for Aerodynamic, Aeroacoustic and Aeroelastic Investigations
TE	Trailing Edge
TEC	Turbine Exit Casing
TEGV	Turbine Exit Guide Vane
TLV	Tip Leakage Vortex
UPV	Upper Passage Vortex

Symbols

Ma	Mach Number
p	Pressure

Subscript

t	Total

Greek

α	Yaw Angle
ω	Angular Velocity

INTRODUCTION

Many investigations have been performed in the past and are still ongoing to increase the efficiency of aircraft engines. One part of the overall engine is the low pressure turbine. A possible way to rise the effectiveness of such components is to decrease the aerodynamical losses. These losses include amongst others also skin friction on the vanes and blades.

A lot of investigations have been performed concerning different surface structures in combination with blade cascades as well as with guiding structures on the surface of flow channels. One of the examined structures are so called riblets, which are grooved microstructures. Using these riblets has shown, that a reduction of skin friction in turbulent flow is possible. Numerous studies about those ribbed structures have been done in the last decades. Investigations concerning the optimum position of the riblets, the range of Reynolds numbers as well as Mach numbers and angles of attack. The best position of the riblets on a vane or blade is not uniform according to different sources in literature. Fang et al. (1990) investigated a compressor cascade with the riblets on the pressure side of the blades, gaining 10% loss reduction. Nagao and Breugelmans (1999) on the other side indicated that riblets increase skin friction when applied on the pressure side of compressor blades. The reason they mentioned is that the Görtler instability increases. They examined a variation of different Reynolds numbers as well as different angles of attack. Lietmeyer et al. (2013) showed an investigation on compressor blades with riblets aligned with the dominating wall shear stress. The outcome was a profile loss reduction of 4% with riblets placed on the suction side. Boese and Fottner (2002) showed the overall loss behavior of highly loaded blades in a compressor cascade. They could achieve a reduction of the pressure loss coefficient of 8% using riblets again on the suction side. Another important parameter influencing the drag reduction is the pressure gradient. Bechert et al (1997) made investigations with zero pressure gradient and Debisschop and Nieuwstadt (1996) with adverse pressure gradient. With the zero pressure gradient a reduction of the friction drag of about 10% was achieved. In the work of Debisschop and Nieuwstadt (1996), they could even show an increased reduction by almost a double compared to the zero pressure gradient measurement.

Miao et al. (2015) presented riblets applied on a turbine blade endwall in a low-speed cascade test section and showed a way to control the endwall secondary flow. The performed CFD calculations were supported by the experimental data and showed that the passage vortex loss core is moved towards the endwall by using riblets.

In literature one can find numerous studies with a clean inflow but none with unsteady effects. It is assumed, that not having a clean inflow leads to a lower value concerning the skin friction reduction compared to a clean one. Viswanath (1999) showed in his work that starting from a certain deviation of the streamline angle compared to the riblets direction, the structure acts like an additional roughness. This deviation is very likely in an unsteady flow field. Therefore, the present work deals now with the use of riblets in a LPT, in which the flow is highly unsteady due to the interaction of vanes and blades as well as due to secondary flow structures.

Therefore, the main goal of this work is to validate a design process for riblets which is also patent. This is done by using a steady numerical simulation to quantify the riblets effect, without the need to model them, instead of using a more time consuming unsteady simulation. The numerical

results are than compared with aerodynamical results, obtained by experiments in a subsonic test turbine facility. Both cases include the ribbed structure on guiding vanes located downstream of a LPT rotor. This comparison shows, that it is possible to design riblets and make a sufficient analysis of them using a less time consuming steady CFD simulation, compared to an unsteady simulation.

RIBLETS EFFECT

Riblets are grooved surface structures which reduce skin friction compared to a smooth surface. One mechanism concerning the skin friction reduction effect is a difference in the virtual origin of the longitudinal flow and the crossflow. This virtual origins, which are indicated by the red dots in Figure 1, are valid under viscous flow conditions and describe an elevation of the velocity profile origin. In this height, the ribbed surface appears as a smooth surface with its origin depending on the type of flow (longitudinal or crossflow) over the riblets. Looking at Figure 1 it can be seen, that the virtual origin of the crossflow is closer to the rib tip than in the case of a longitudinal flow. Shear stresses of the crossflow increase because of this smaller distance. With this higher crossflow resistance compared to the longitudinal direction, the fluid is moving more in the latter one. This leads to a reduction of the crossflow fluctuations, which is resulting in a lower momentum transfer, i.e. it is reducing the vertical motion. The reduction of this motion is then in the end decreasing the shear stresses and skin friction.

A second mechanism for reducing skin friction is a limitation of the surface area which is interacting with streamwise vortices. Although increasing the wetted surface by using riblets, the spacing between the riblets can be chosen in a way that the mentioned vortices are only interacting with the rib tips. This happens if the size of the vortices is bigger than the distance between two riblet tips. In this case the skin friction is lower compared to the absence of the ribbed surface structure (see also Choi et al. (1993)).

The optimum skin friction reduction can be achieved if the riblets are aligned with the freestream direction. A more detailed description of the mechanism can be found e.g. in Bechert et al. (1997).

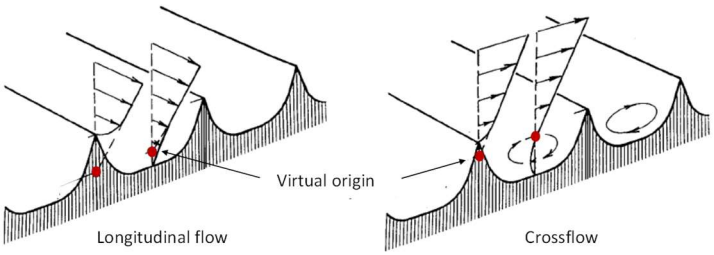

Figure 1: Viscous longitudinal and crossflow on a ribbed surface - Bechert et al. (1997)

EXPERIMENTAL FACILITY

The Institute of Thermal Turbomachinery and Machine Dynamics at Graz University of Technology operates a 3MW compressor station in order to supply a couple of test facilities continuously with pressurized air. The maximum mass flow rate is 15 kg/s at a stage inlet temperature of 100°C. This inlet temperature can be adjusted by coolers within a wide range. The pressurized air enters the facility, which is shown in Figure 2, through a spiral inlet casing where the flow turns from radial into axial direction. In order to provide well defined and uniform inflow conditions a de-swirler together with a perforated plate is located upstream of the stage inlet. Downstream of this perforated plate, inlet guide vanes can be found which should simulate additional wakes of other upstream low pressure turbine stages. The LPT stage itself contains of an unshrouded rotor with a flat rotor tip. The air leaves the rig through an acoustic measurement section, supporting struts, exhaust casing, and the exhaust stack to ambient. A detailed description of the subsonic test turbine facility for aerodynamic, aeroacoustic, and aeroelastic investigations (STTF-AAAI) is given in Moser et al. (2007).

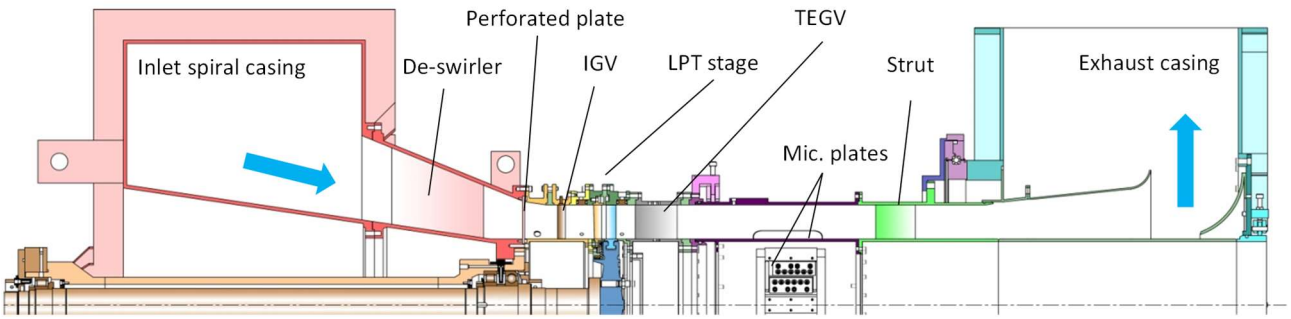

Figure 2: Experimental facility STTF-AAAI

Operating Point

Table 1 shows geometrical details of the investigated LPT stage as well as the conditions for the selected operating point. The Reynolds number of the vanes is defined by using the midspan conditions of the rotor exit as well as the axial chord of the vanes.

Turbine Exit Guide Vanes

The TEGV's have already been tested successfully during other projects but without any foil on their surfaces. For the study in this work they were equipped with riblets on the suction side. Results of those vanes with riblets are shown and compared with CFD calculations which were performed before the experimental tests. With these simulations, the designing of the later used riblet foil for the theoretical conditions in the LPT stage was done.

Table 1: Operating conditions and geometrical details

Operating Conditions		Geometry details	
TEGV Reynolds number	~340000	Number of blades/vanes	
Stage pressure ratio	1.16	IGV/Stator/Rotor/TEGV	83/96/72/15
Corrected speed	4042 rpm		
Corrected mass flow rate	6.94 kg/s	Tip gap to blade height ratio	1.0%
Stage total inlet temperature	100 °C	Hub to tip radius ratio	~2/3

Figure 3 shows a vane with the riblet surface on the suction side, which can be identified due to the shimmer of the surface. In the area between the leading edge (LE) and the red line in Figure 3 as well as on the TEGV's pressure side, a smooth foil was applied. The reason to start with the riblets a little bit downstream of the LE is that the turbulent flow starts in the area which is indicated by the mentioned red line. Also Lietmeyer et al. (2013) stated in his work, that the profile losses are significantly higher with riblets starting already from the leading edge. To avoid the flow hitting a forward facing step between the riblet foil and the vane surface, the smooth foil was also used in a small part of the suction side.

Additionally, the orientation of the riblets is shown in the small picture in Figure 3. with the tips in grey and the valleys in black. Surface streamlines (from CFD prediction) can be seen in Figure 4. In addition, it shows the ideal riblet size according to a proprietary algorithm described in the EU patent no. EP 2261117 A2. It can be seen that for an optimal use, the riblets size should be varied along the span. In general, riblets have to be located inside the buffer layer. If their tips reach into the turbulent layer they act like an additional surface roughness. The ideal riblet tip distance has to be determined experimentally and can then be converted with dimensionless sizes and other fluid and flow conditions. With a tip distance of 45 µm or 90 µm, two different sizes of riblet structures were available concerning the test runs in the STTF-AAAI. The selected geometry of the chosen riblets is a trapezoid type with 45 µm tip distance and a height to tip distance ratio of 0.45. These dimensions are uniform over the whole span. According to the CFD result, the angle of the streamlines is about 10 deg at the vane surface. Therefore, the realized angle of the riblets at the overall suction side was equally to that. A variation of ±10 deg is in the toleration of the riblets, what was also mentioned in

Viswanath (1999). In case of higher angle deviations, the foil would work as a surface roughness and increase the wall shear stress.

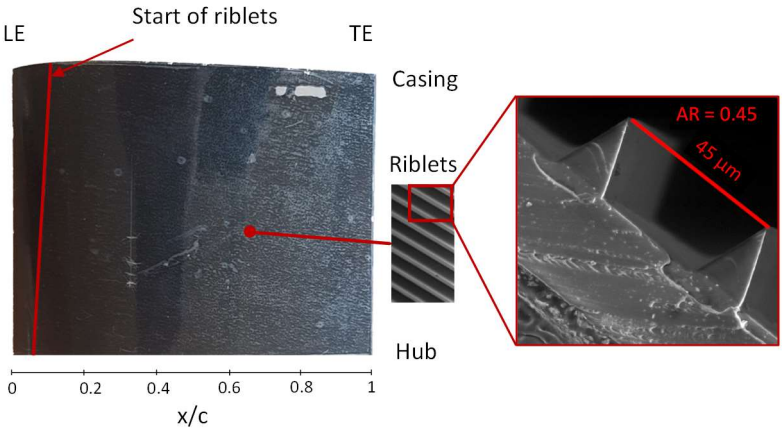

Figure 3: TEGV with riblets on the suction side

Measurement Techniques

In order to determine the aerodynamic flow field up- and downstream of the investigated configuration, steady flow field measurements using a five-hole-probe as well as a trailing edge probe have been performed over a TEGV pitch.

The used trailing edge probe was a simple pitot pipe for measuring the total pressure downstream of the vanes, with a probe head diameter of 80% related to the trailing edge thickness. The distance between the trailing edge of the vanes and the measurement plane was 0.3mm. This small gap ensured that the wake was not yet fully mixed out before the inlet of the probe. The resolution of the measurement was 0.2 deg, or 0.83% of a TEGV pitch, between two following points, what results in 120 measurement points in circumferential direction.

Steady measurements, using a five-hole-probe (probe head diameter of 2.5mm or 250% of the trailing edge thickness) from the Institute of Jet Propulsion and Turbomachinery, RWTH Aachen University, have been performed in a plane downstream of the rotor and in a plane downstream of the TEC, which are marked with C and D in Figure 5a. The spatial resolution was 0.312% of a vane pitch in circumferential direction. One radial height consisted of 21 measurement points. Table 2 shows the radial measurement grid of the five-hole-probe in percent of the channel height.

Table 2: Radial measurement grid for the 5-hole-probe in % of the channel height

4.125	6.375	8.875	13.875	18.875	23.875	28.875
33.875	38.875	43.875	48.875	53.875	58.875	63.875
68.875	73.875	78.875	83.875	88.875	92.625	95.125

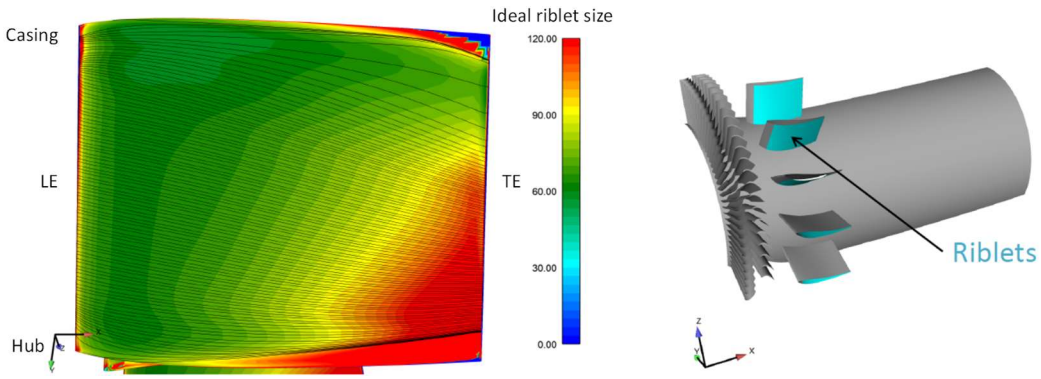

Figure 4: Ideal riblet size (left) and applied regions of the vanes (right)

The size of the measurement sectors in each plane was 24 deg, what corresponds to one TEC pitch. The sectors are shown in Figure 5b, with examples of a measured flow field. On the left side of Figure 5b a measurement in plane C (downstream of the rotor) is shown with a sketch of the stator located upstream of the plane. On the right side, a measurement in plane D (downstream of the TEC) is shown. Both pictures are aft looking forward to the inlet of the test rig. Plane C is located in a distance of 60% related to the rotor blade chord length downstream of the rotor trailing edge and Plane D is located 108% related to the TEGV chord length downstream of the TEGV trailing edge.

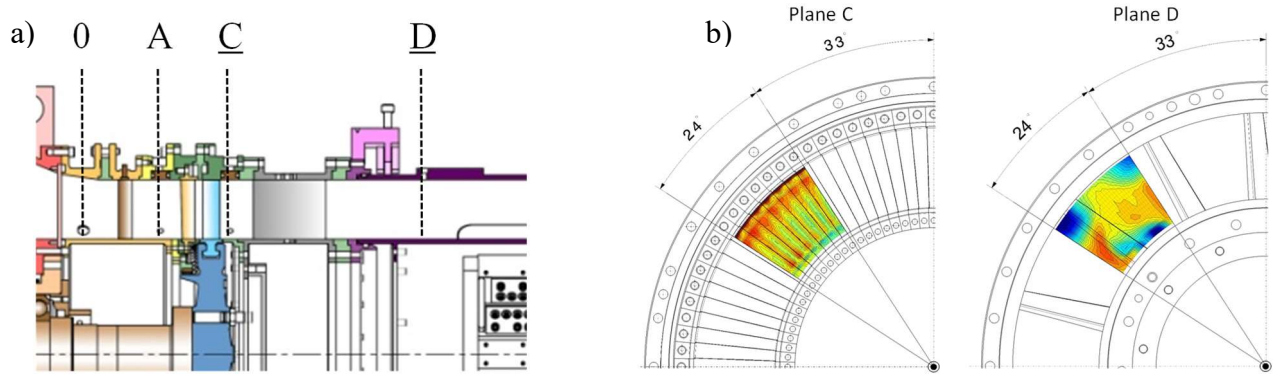

Figure 5: Measurement planes (a) and measurement sectors (b)

To see the possible influence of a different surface onto an upstream located LPT rotor, blade vibrations measurements have been performed by means of strain gauges located on different rotor blades. More details concerning the positioning of the strain gauges and the exact measurement procedure can be found in Simonassi et al. (2018).

Measurement Uncertainty

The measurement system is made up by eleven multi-channel pressure transducers PSI 9016 with a total amount of 176 channels and an accuracy of 0.05% full scale and four National Instruments Field Point FP-TC-120 eight-channel thermocouple input modules and one FP-RTD-122 resistance thermometer input module.

Table 3 shows the measurement uncertainties (within a 95% confidence interval) of the five-hole-probe measurements. These values are positive and negative deviations and contain the error due to the approximation, random error and the systematic error of the PSI Modules. The difference between the positive and the negative direction is a result of the multi-parameter approximation.

The sensor signal amplifier of the telemetry system has a zero drift of 0.02%/°C and an accuracy of linearity of 0.1%. The strain gauge resistance is 350Ω±0.3% with a gauge factor of ±1.0%, a transverse sensitivity of 0.0% and a temperature coefficient of gauge factor of 101±10 [10^{-6} /K]. The temperature on the blade surface was measured aby applied high precision fine wire thermocouples of type K, in order to take temperature compensations into account.

The variation of speed is below 0.2% of the current operating speed. The measurement uncertainty of the temperature measurement is about ±0.5K.

Table 3: Measurement uncertainties of the five-hole-probe

Ma	+0.006	-0.003	[/]
α	+0.5	-0.08	[deg]
p_t	+3.3	-3.0	[mbar]
p	+5.3	-5.2	[mbar]

NUMERICAL SET-UP

A steady-state Reynolds-averaged Navier-Stokes (RANS) simulation was performed during the numerical investigations by using the commercial solver ANSYS® Fluent® v15.0. As turbulence model, the k–ω SST model was chosen with a turbulence intensity of 6% and a correlated hydraulic diameter of 0.39m. The used solver was pressure based. In order to take the rotation of the LPT rotor into account, this component was defined as a rotating zone using MRF (Multiple-Reference-Frame). Using this MRF approach led to a solution for the moving cells concerning the moving reference frame equations. Steady zones were simply solved by using the stationary forms of the equations. This approach is equal to a frozen rotor formulation which means that the result is a steady-state simulation for one position of the rotor zone.

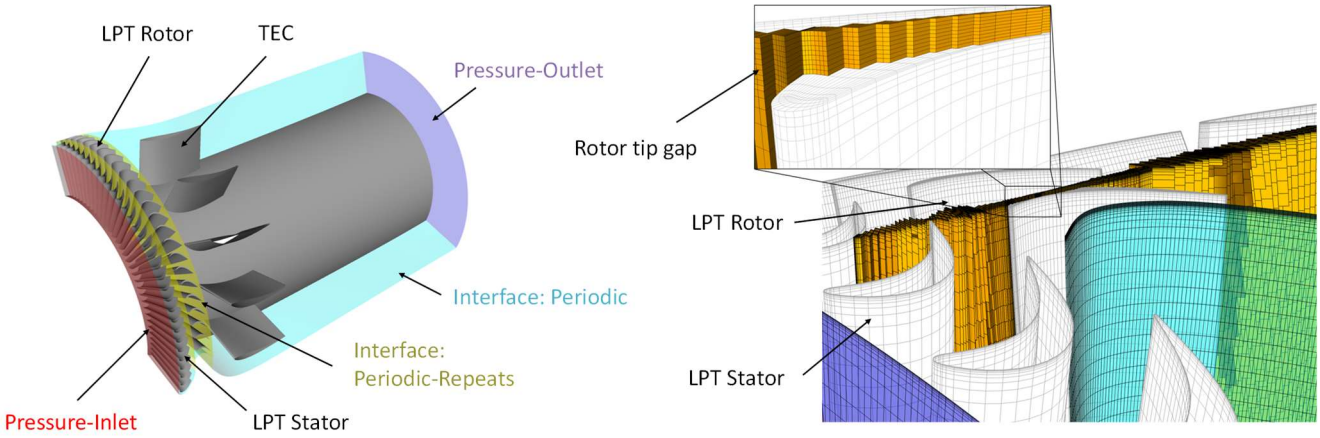

Figure 6: Simulation domain (left) and mesh detail between blade tip and outer casing (right)

For the simulation, only a part of the whole test rig was defined as the domain, starting right upstream of the LPT stator (in a distance of 10% of the stator chord length) and ending downstream (in a distance of 424% of the TEGV chord length) the microphone plates (see Figure 2), containing the LPT stage and the TEC (see Figure 6 left). With that chosen numerical domain, the obtained results could be observed with the right accuracy. To realize periodic boundary conditions as well as to minimize the mesh size and computational time, the inlet guide vanes upstream of the LPT stage were not taken into account in the simulation. Full periodicity was achieved by selecting a 120 deg sector of the full flow channel. The numerical mesh was generated with ANSYS® ICEM® and consisted of block-structured cells with three cell zones and a total amount of around 16.1 million cells and 16.7 million nodes. The number of cells and nodes were verified by a mesh sensitivity study. Table 4 shows the number of cells and nodes for each zone.

Table 4: Number of cells and nodes

	Number of cells	Number of nodes
Stator	2.414.720	2.554.496
Rotor	7.685.928	8.002048
TEGV	6.003.800	6.173.888
Total	**16.104.448**	**16.730.432**

Figure 6 shows on the right side the 0.5 mm gap between the blade tip and the channel outer casing which has been resolved with 9 cells. At each wall of the domain, the near wall y^+ values were smaller than 5. The boundary layers were modelled fully turbulent. Experimental data was used as inlet (total pressure and temperature, yaw and pitch angle) and outlet (static pressure) conditions. As a fluid, air was defined according to the ideal gas law. The dynamic viscosity was calculated according to Sutherland's Law, which implies a temperature-dependency.

According to the mentioned patent the riblets have not to be modelled in a CFD simulation what would require a much finer mesh. The effect of the riblets can simply be correlated from a smooth

surface. This leads to the same aerodynamical behaviour but without an additional modelling of the grooved micro structure.

RESULTS AND DISCUSSION

As already mentioned in the section before, the CFD calculation was performed with a MRF approach. Therefore, the contour plots shown in the following section can't be compared directly but are stated for a first information about the flow field. The direct comparison of the comparable circumferential averaged results is shown later in this work. All plots in this section concerning the flow fields downstream of the rotor as well as downstream of the TEC show three different aerodynamical parameters. The total pressure on the left side, the Mach number in the middle and the yaw angle on the right side. All three pictures are aft looking forward. The used colourmap is the same for the numerical as well as for the experimental results where blue stands for a low value of the examined flow parameter and red for a high one.

Numerical Results

Rotor Exit Flow

In Figure 7 the results of the CFD simulation in plane C are shown and are presented in the rotor frame. Because of calculating the system with a MRF, one can see the wakes, indicated with black dashed lines, of the rotor blades and not of the stator vanes like in the case of the experimental results (steady vane frame) (see Figure 10). The pressure side (PS) is on the left side of the wake and the suction side (SS) on the right side. Clearly visible is the tip leakage vortex (TLV) due to the rotor tip, indicated by the lower values of total pressure and Mach number at around 90% of the channel height. From the very hub up to around 15% channel height, secondary flow effects can be observed. ω indicates the rotational direction of the LPT rotor.

TEGV Exit Flow

Figure 8 shows the simulated flow field of the TEGV exit wherein three vortices can be identified. A smaller one (A) on the outer casing, rotating in counter clockwise direction, on the suction side of the TEGV, a big vortex (B), rotating in clockwise direction, on the pressure side and another small one (C) on the inner casing. Figure 9 depicts the origins of the two vortices located on the outer casing according to the CFD simulation. Inflow as well as outflow direction of the TEC are indicated by white arrows and the TEGVs are coloured in grey. Red colour stands for a negative direction of rotation and blue for a positive one. The smaller vortex, which is again marked with (A), is caused by a separation on the suction side and the bigger one, which is marked with (B), results from a separation on the pressure side. Separation (B) is additionally shifted in the direction of the neighbouring vanes suction side due to the pressure gradient between the two vanes. The latter one can also be identified in picture (3) of Figure 14, which shows an oilflow visualization of the TEGV pressure side. The vortex at the hub, marked with (C), is assumed to be the lower passage vortex (LPV).

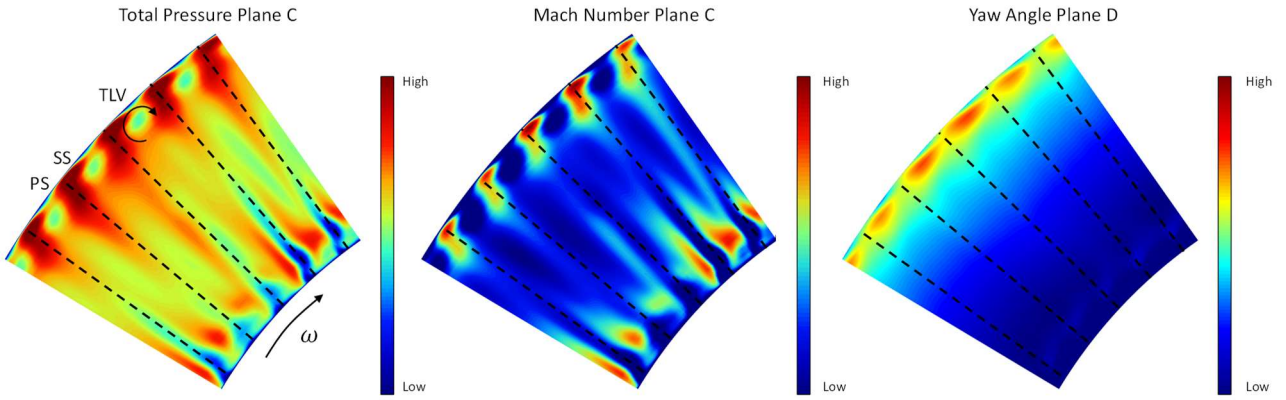

Figure 7: Flow field – Rotor exit – Simulation

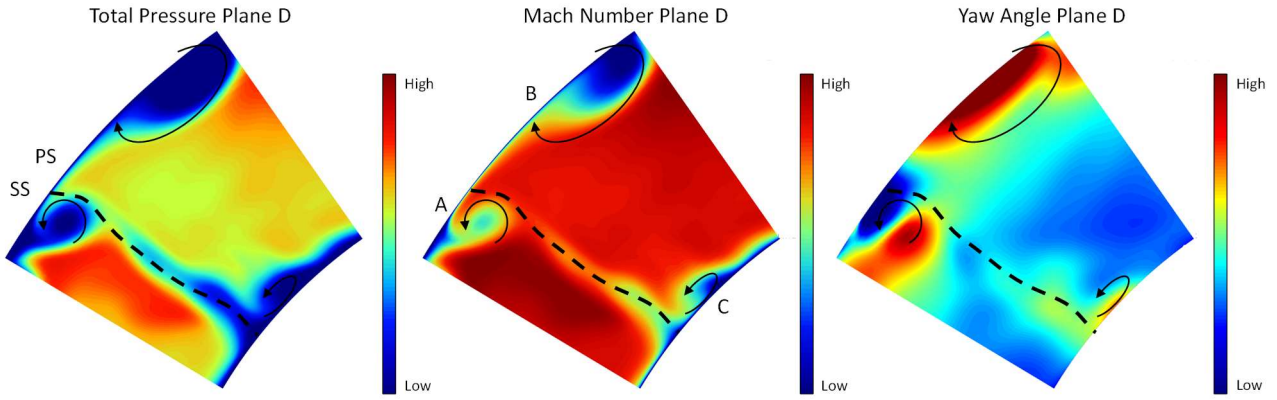

Figure 8: Flow field – TEC exit – Simulation

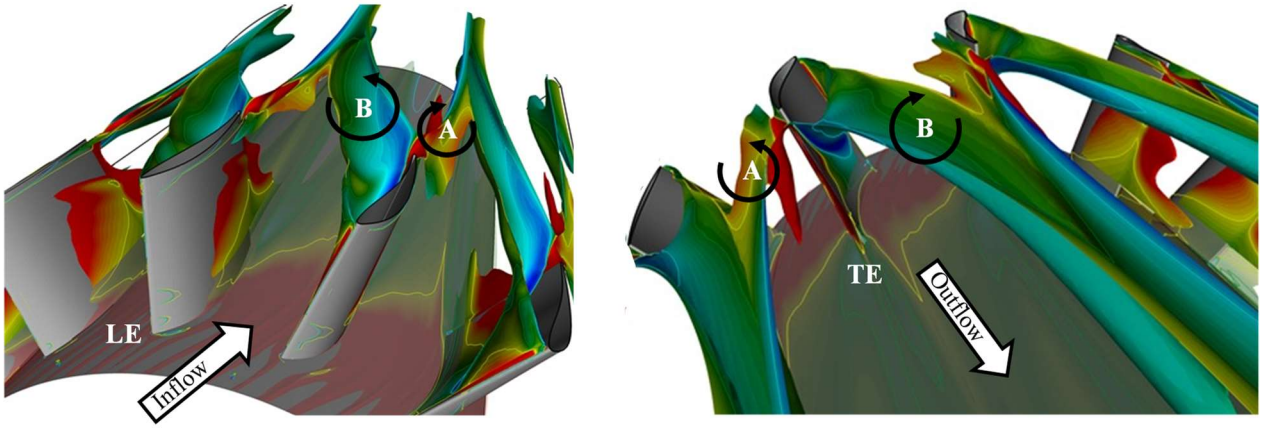

Figure 9: Origin of vortices at the casing in plane D

Experimental Results

Rotor Exit Flow

Figure 10 shows the rotor exit flow, which is equivalent to the inlet flow of the TEC. ω is again indicating the rotational direction of the rotor. The dashed black lines show the wakes of the upstream of the rotor located stator vanes. Radial structures are due to upstream located static vanes (LPT stator) and the moving rotor whereas circumferential patterns are due to the stator. As already seen in the numerical results, the lower values of total pressure and Mach number as well as the high values of the yaw angle in the region close to the outer casing indicate the tip leakage vortex of the rotor (marked with A). High values of Mach number and total pressure at the very casing indicate a jet caused by the rotor tip gap (marked with B). This tip gap and the resulting tip leakage vortex is causing the already mentioned separation on the pressure side of the downstream located TEGV (marked with (B) in Figure 9). The reason is that the TEGV is operating at positive incidence in the region close to the tip as was already seen by Selic (2015).

The region between hub and about 15% of the channel height (marked with C) is dominated by secondary flows which result from the upstream located stator, the rotor itself and from the interaction of these two vane rows.

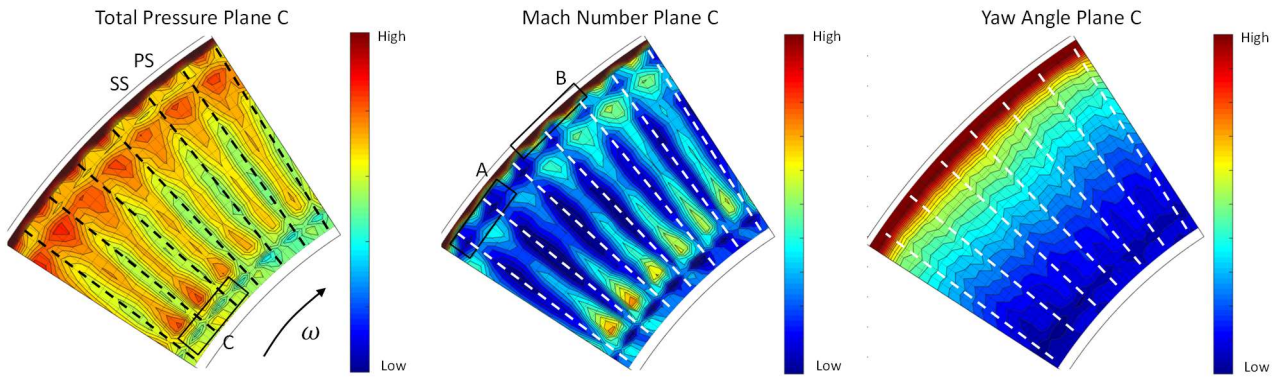

Figure 10: Flow field - Rotor exit – Measurement

TEGV Exit Flow

Figure 11 shows the exit flow of the TEGV. The black dashed line indicates the wake of a vane with the pressure side on the right and the suction side on the left side of the line. Two vortices can be clearly identified in this measurement. The upper passage vortex (UPV) on the casing and the lower passage vortex (LPV) on the hub. One can see that the wake of the vane is skewed due to these vortices. The UPV in the measurement extends over a wider area on the casing compared to the simulation. Also the smaller red spot at the outer casing in the yaw angle is assumed to be a part of the UPV.

Comparison

As already mentioned above, the flow fields of the simulation and the experiments can't be compared directly. Therefore, an averaging in circumferential direction of the measurement field had to be done. Figure 12 shows the radial distribution of the massaveraged total pressure, Mach number and yaw angle for both measurement planes. The simulation is drawn with a dashed line and the experiment with the continuous line including the radial measurement points shown by black marks. A limitation of the results obtained by the simulation was done intentionally, to compare only the part of the flow field which could also be measured.

In the rotor exit field (plane C), the results are of good agreement although there is a small offset over the whole radial height for each parameter. The biggest deviations are at hub and casing, where the vortices are located. When comparing the yaw angle distribution in plane C, it can be seen that the simulation predicts a smaller value due to the tip leakage then the experiment showed. In this region, the over and underturning in the experiment is higher than in the simulation. Looking at the Mach number distributions, it can be seen that a loss core of the experiment is located at 90% relative channel height and therefore a little bit lower compared to the position at 95% in the simulation.

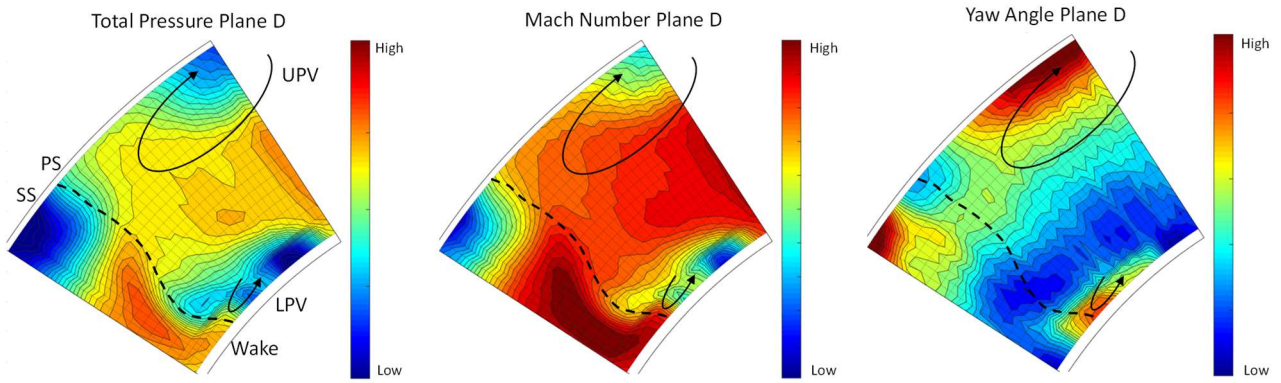

Figure 11: Flow field - TEC exit - Measurement

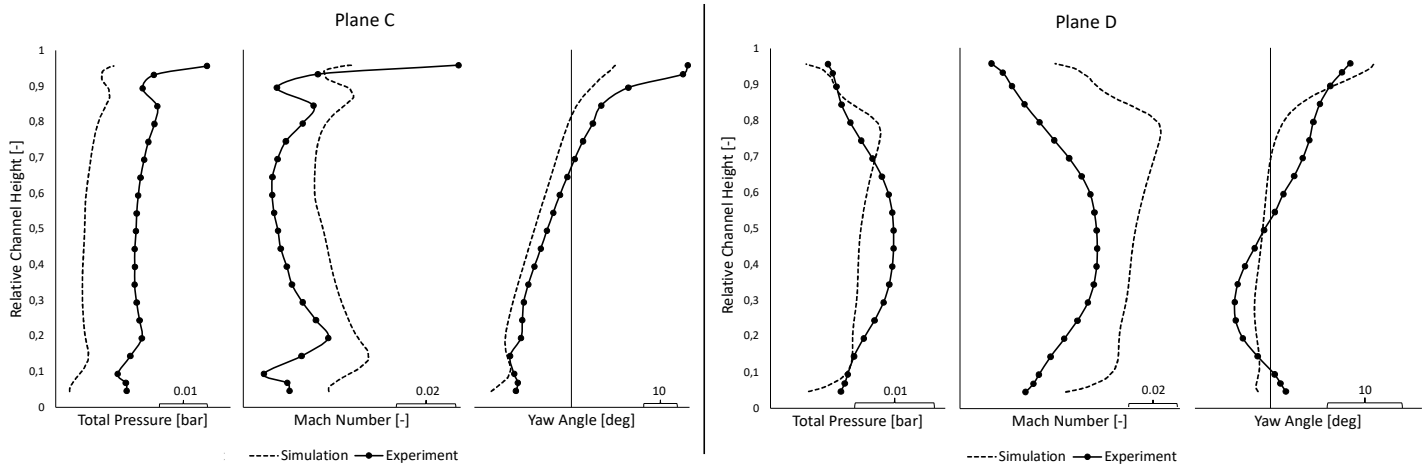

Figure 12: Radial distribution of aerodynamical parameters; Plane C (left) and Plane D (right)

By comparing the distributions in plane D, one can see a difference in the shape between the simulation and the experiment but in overall the results agree very well. In the experiment, the flow in this measurement plane is already mixed out more compared to the simulation, which leads to the deviations in the regions of the inner and outer casing. In the yaw angle distribution at around 90% of the relative channel height, it can be seen that the over and underturning is higher in the simulation compared to the experiment.

By comparing Figure 8 and Figure 11 one can see the same difference in the size of the UPV and LPV respectively. In the region between 10 and 70% of the channel height, which is dominated by the 2d-interaction between the rotor and the TEGV, the simulated flow field doesn't fully match the measurement but is within a range of good agreement.

The offset in total pressure between the experimental and numerical result is 0.94% for plane C and 0.13% for plane D based on the total inlet pressure.

Trailing Edge Results

Figure 13 shows the results of the trailing edge measurement and simulation normalized by their mean values. On the ordinate the total pressure is shown and on the abscissa the circumferential position can be seen. The position is from 0 to -24 deg because the measurement was taken in counter clockwise direction of the rotational direction of the rotor. This is also the reason why a negative sign was chosen. The measurement positions are again indicated by the black marks. One can clearly see the drop in total pressure which indicates the position of a wake. The pressure side of the vane is indicated by PS on the right side of the wake and the suction side is on the left side indicated by SS. There is a slight shift concerning the location of the minimum in total pressure of about 0.5 deg between the simulation and the experiment. That means a very good agreement between both results concerning the circumferential position. The whole distribution of the simulation is shifted to slightly smaller values of total pressure, what can be explained by the dependency onto ambient conditions of the experiment. Because the test rig is an open loop machine, there is a difference in the absolute values during an experiment. Concerning the setting of the operating point, relative values (m_{corr}, n_{corr}, stage pressure ratio) are adjusted. This leads to an aerodynamic identical operating point.

The wake width, calculated according to the work of Schobeiri and John (1996), is in the case of the simulation 0.0029 m and in the case of the experiment 0.0026 m. Looking at the associated momentum thickness of the wake, the values are 0.00104 m for the experiment and 0.00109 m for the simulation.

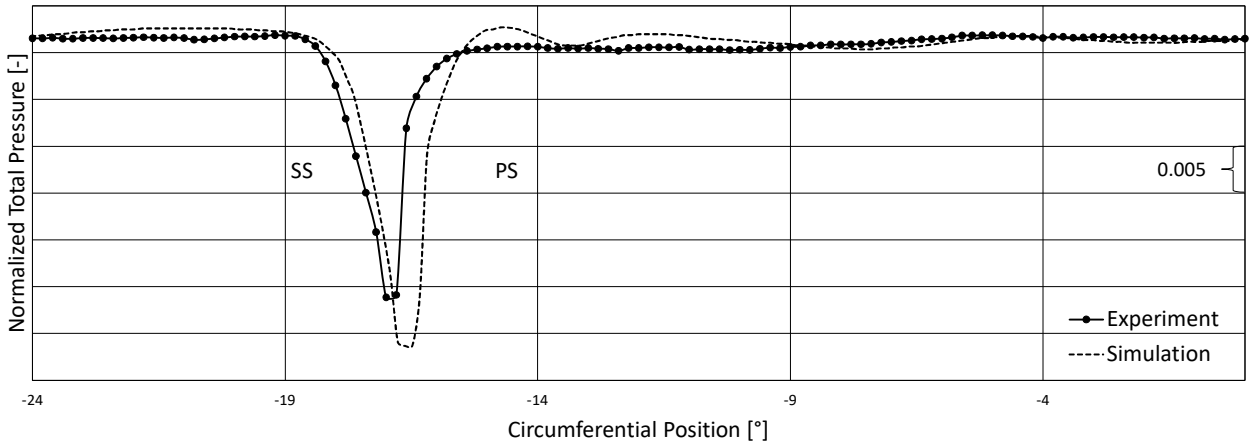

Figure 13: Total pressure distribution downstream of the trailing edge

Oilflow visualization

Figure 14 shows four results (for a qualitatively visualization) of two different oilflow visualization test runs. Pictures (1), (2) and (3) represent vanes with riblets and (4) shows a case of the same vanes but without riblets. The red line marked with (A) in picture (1) and (2) indicates again the start of the riblets on the surface of the vane.

In the case of (1), (3) and (4), the whole vane was covered with oil while in picture (2) only some spots on the LE of one vane were marked. The difference between the two outer pictures (1) and (4) is the viscosity of the oil. For (1) a different viscosity was chosen to see if the riblets are also influencing the boundary layer further away from the vane surface.

When comparing the images (1) and (2) one can clearly see that the riblets are only influencing the lower boundary layer. In (2) the oil is perfectly following the direction of the riblets over the biggest part of the suction side (indicated by the orange lines and marked with (B)) whereas in (1) these streamlines are not visible. This can be seen by comparing pictures (2) and (4) were the viscosity is identical. In (4) the streamlines, marked with (C), are skewed in direction of the TE due to secondary flow effects, while in picture (2) it can be clearly seen that the indicated orange lines (B) are parallel.

In picture (1), the viscosity of the oil is higher and therefore the influence of the riblets is not visible. But when comparing it with Figure 4 and picture (4) in Figure 14Figure 10, one can see the same behaviour of the flow. In both cases, the flow moves radially inwards due to the pressure gradient (indicated by black lines marked with (E) in Figure 14 (1) and the white lines marked with (C) in picture (4)).

As already mentioned in the section with the numerical results for the TEGV exit flow, Figure 14 (3) depicts a separation on the pressure side of the vane, indicated by the dashed line and marked with (D).

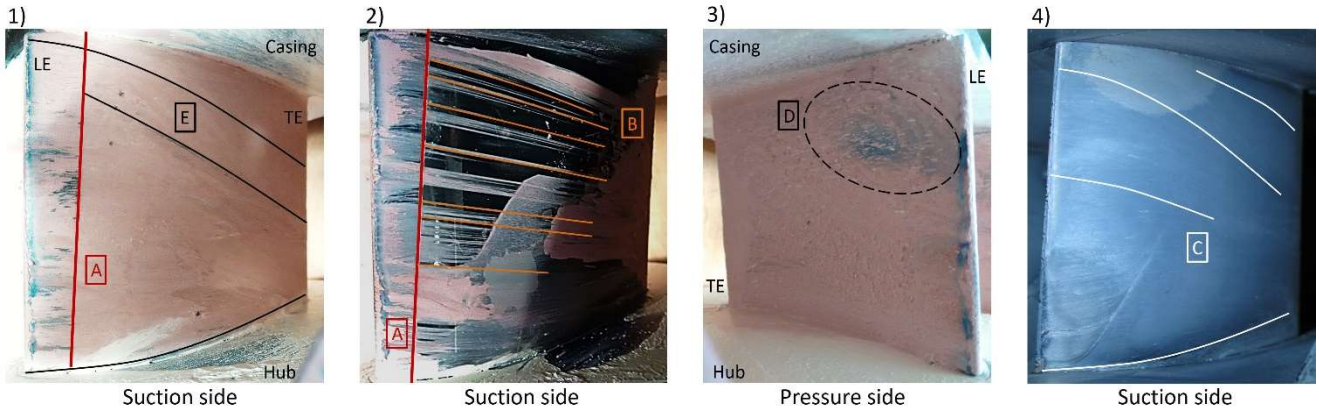

Figure 14: Oil flow visualization: Riblets (1,2 and 3), no riblets (4)

Rotor Vibrations

To see if the riblets and therefore the changed surface structure has any influence onto the upstream located LPT rotor blade vibrations, strain gauge measurements have been performed. A comparison is done with measurements taken before this testing campaign with the same vanes but without riblets. Figure 15 shows a strain gauge result concerning the vibration amplitudes. In black the case with no foils on the TEGV's is depicted and red shows the result with riblets on the vanes suction side. One can see that the amplitude of the frequency close to 1000 Hz, which is the first eigenfrequency (1st flapwise bending mode) of the rotor blades, is smaller for the set-up without riblets. The same result is also visible for the other strain gauges, which are not shown in this work. The authors assume that a change in the upstream potential effect is causing a change in aerodynamic damping or excitation force, thus reducing the vibration amplitude. It should be mentioned, that this eigenfrequency is due to an excitation by the rotor – TEC interaction (see Schönleitner et al. (2016)). At 2000 Hz and 3000 Hz are the second (1st edgewise bending mode) and third (1st torsion mode) eigenfrequencies but there is not much of a change concerning the vibration amplitudes. A higher response amplitude can be caused by a stronger excitation and/or less damping. Which in this case is more or less a change in aerodynamic damping. Material and structural damping is exactly the same for both measurements (same rotor, same operating point).

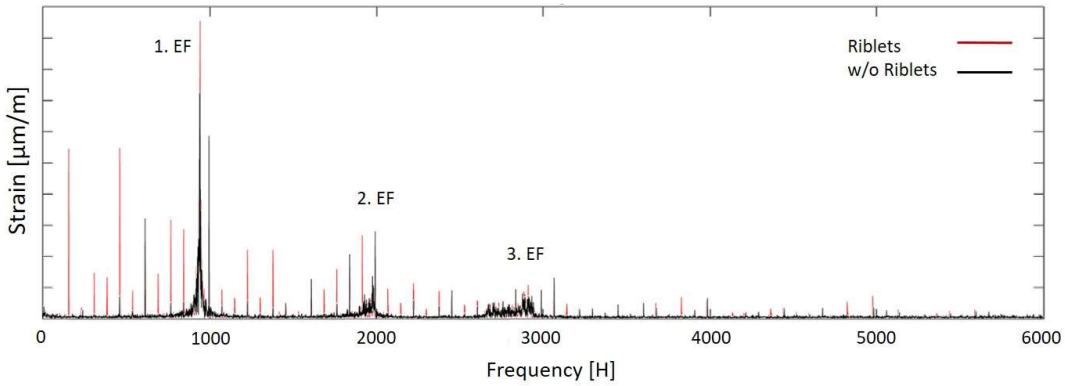

Figure 15: Vibration amplitude

CONCLUSIONS

A comparison of results obtained by numerical and experimental investigations of a 1 ½ stage low pressure turbine with riblet structures applied on the suction side of the turbine exit guide vanes has been performed. The aerodynamical results show a good overall agreement when comparing the exit flow field of the rotor. Looking at the TEGV outlet flow, a bigger difference, especially in the regions of the inner and outer casing, can be observed. A possible reason is that in those areas big vortices occur, what can also be seen from the results. The simulation is then underpredicting the mixing of the flow. But in total, also these results have a good agreement. A comparison of the wake 0.3 mm downstream of the TEGV trailing edge showed also a good agreement. There is a small shift of the total pressure minimum in the circumferential direction (0.5 deg), which can be explained by the uncertainty concerning the mounting of the trailing edge probe. Additionally, vibration measurements of the LPT rotor blades using strain gauges have been performed. After comparing a set-up with riblets and one without a foil on the TEGV's, a small increase of the vibration amplitude of the rotor blades first eigenfrequency can be observed in the case with riblets.

The main conclusion is now, that the results of the steady state simulation and the unsteady experiment have a very good accordance. Therefore, a more time consuming unsteady simulation is not necessarily needed to predict the behavior of a riblet structure in a LPT stage designed according to the cited patent. It should again be mentioned, that with this approach it is not necessary to model the investigated micro structure. A modelling of them would require a much finer mesh; hence the computational effort would also be much higher. That means that a steady state numerical simulation excluding riblets can predict their behavior in an unsteady experimental case in a very good way.

ACKNOWLEDGEMENTS

The authors thank Dr.techn. H.P. Pirker for operating the compressor station and his great support and discussions during all experimental investigations.

This work has been carried out in the framework of the national funded TAKE-OFF programme within the research project hallstaTt (contract no. 850444) regarding sound power reductions of low pressure turbine by means of modifications on the turbine exit guide vanes at Graz University of Technology at the Institute of Thermal Turbomachinery and Machine Dynamics. The authors therefore thank the Austrian Research Promotion Agency (FFG) and the Austrian Ministry for Transport, Innovation and Technology (bmvit) for funding this project.

REFERENCES

Bechert, D., Bruse, M., Hage, W., Van der Hoeven, J., & Hoppe, G. (1997). *Experiments on drag-reducing surfaces and their optimization with an adjustable geometry*. J. Fluid Mech. Vol. 338, pp. 59-87.

Bechert, D., Bruse, M., Hage, W., & Meyer, R. (1997). *Biological Surfaces and their Technological Application - Laboratory and Flight Experiments on Drag Reduction and Separation Control.* AIAA 28th Fluid Dynamics Conference

Boese, M., & Fottner, L. (2002). *Effects of Riblets on the Loss Behavior of a Highly Loaded Compressor Cascade*. Proceedings of ASME Turbo Expo 2002, Amsterdam, Netherlands.

Choi, H., Moin, P. & Kim, J. (1993). *Direct numerical simulation of turbulent flow over riblets.* Journal of Fluid Mechanics. Vol. 225, pp. 503-539

Debisschop, J., & Nieuwstadt, F. (1996). *Turbulent Boundary Layer in an Adverse Pressure Gradient: Effectiveness of Riblets*. AIAA Journal Vol. 34(5), S. 932-937.

Fang, C., Yan-Ping, T., & Mao-Zhang, C. (1990). *An Experimental Investigation of Loss Reduction with Riblets on Cascade Blade Surfaces and Isolated Airfoils*. Gas Turbine and Aeroengine Congress and Exposition, Brussels, Belgium.

Leitl, P. A. (2010). *European Patent No. EP2261117A2.*

Lietmeyer, C., Ohlert, K., & Seume, J. (2013). *Optimal Application of Riblets on Compressor Blades and Their Contamination Behavior*. Journal of Turbomachinery Vol. 135(1).

Miao, X., Zhang, Q., Wang, L., Jiang, H., & Qi, H. (2015). *Application of Riblets on Turbine Blade Endwall Secondary Flow Control*. Journal of Propulsion and Power, Vol. 31, No. 6.

Moser, M., Kahl, G., Kulhanek, G., & Heitmeir, F. (2007). *Construction of a Subsonic Test Turbine Facility for Experimental Investigations of Sound Generation and Propagation for Low Pressure Turbines.* Beijing, China.

Nagao, S., & Breugelmanns, F. (1999). *Investigations of Riblets in a CDB, DCA and 65-S Compressor Cascade*. Proceedings of International Gas Turbines Congress, Kobe, Japan.

Schobeiri, M.T., & John, J. (1996). *A Study of the Development of Steady and Periodic Unsteady Turbulent Wakes Through Curved Channels at Positive, Zero, and Negative Streamwise Pressure Gradients, Part I.* NASA Contractor Report 198448.

Schönleitner, F., Selic, T., Schitter, C., Heitmeir, F., and Marn, A. (2016). *Experimental Investigation of the Upstream Effect of Different Low Pressure Turbine Exit Guide Vane Design on Rotor Blade Vibration.* Proceedings of ASME Turbo Expo 2016, Seoul, South Korea

Selic, T. (2015). *Experimental Investigation of the Aerodynamics and Acoustics of Exit Guide Vanes for Future Aircraft Engines.* PhD Thesis, Graz University of Technology

Simonassi, L., Benauer, R., Zenz, M., Leitl, P., & Marn, A. (2018). *Numerical and Experimental Study on the Influence of Inlet Distortion on the Aeroelastic and Aerodynamic Performances of a Low Pressure Turbine.* 23rd Blade Mechanics Seminar, Winterthur, Switzerland.

Vishwanath, P. (1999). *Riblets on Airfoils and Wings: A Review*. 30th AIAA Fluid Dynamics Conference, Norfolk, VA.